PAPER

Check for updates

A hybrid YSZ/SnO$_2$/MEMS SO$_2$ gas sensor

Ting-Jen Hsueh [ID] *[a] and Chun-Liang Lu[b]

This study uses a solid YSZ electrolyte film in a SnO$_2$ MEMS SO$_2$ gas sensor of the semiconductor type to enhance the redox reaction. The YSZ film is prepared by RF sputtering. XRD analysis shows the presence of the (111), (200), (220) and (311) peaks that denote the crystallization planes of YSZ. The experimental results show that the SnO$_2$ MEMS SO$_2$ gas sensor with a YSZ film has a better sensor response than a pure SnO$_2$ MEMS SO$_2$ gas sensor or a YSZ MEMS SO$_2$ gas sensor when the SO$_2$ concentration and the sensor's temperature sensors are 250 ppb and 400 °C, respectively. The YSZ/SnO$_2$ sensor's measured responses are around 6%, 45%, 20% and 16% when the sensor is respectively operated at 250 °C, 300 °C, 350 °C, and 400 °C.

Introduction

As technological advances and industrial development are becoming more rapid in the petrochemical industry, environmental pollution has become an important issue. The types of air pollutants include nitrogen oxides (NO$_x$), sulfur oxides (SO$_x$) and PM2.5 (particulate matter with a diameter of 2.5 μm or less).[1] SO$_x$ causes acid rain, soil acidification and climate change.[2] SO$_x$ become PM2.5 when molecules of SO$_x$ react with basic compounds in the atmosphere.[2,3] In the family of SO$_x$ (such as SO, SO$_2$, SO$_3$ etc.), sulfur dioxide (SO$_2$) is a major component, and is usually the indicator that is used for SO$_x$ monitoring.[4] SO$_2$ is one of the most toxic substances known. It is known that toxic gases are hazardous to human health.

Over the past decade, toxic gases have been detected using electrochemical, catalytic bead, photoionization, infrared point and semiconductor devices. The electrochemical type can be divided into those that use liquid electrolytes or solid-state electrolytes. Solid electrolytes are widely studied because they are accurate and reliable, small and light, flexible to install and easy to use.[5] Yttria stabilized zirconia (YSZ) devices have high chemical and thermo mechanical stability.[6] For thick film applications, the operating temperature of the YSZ is more than 600 °C.[6]

Recently, the authors reported a SnO$_2$ micro-electro mechanical systems (MEMS) gas sensor.[7] Semiconducting metal oxide MEMS gas sensors have a number of advantages in terms of use in consumer devices, such as low cost, high efficiency, high integration, low power consumption, high sensitivity and being well suited to wearable applications. They are potentially compatible with silicon microelectronics. The oxygen-related gas-sensing mechanism involves the absorption of oxygen molecules on the oxide surface to generate chemisorbed oxygen species (O$_2^-$, O^{2-}, O$^-$) by capturing electrons from the conductance band, which makes the oxide surface highly resistive. The oxide is exposed to traces of the reductive gas. In reacting with the oxygen species at the oxide surface, the reductive gas reduces the concentration of the oxygen species on this surface and thereby increases the electron concentration.[8] However, SO$_2$ molecules have an indistinctive redox reaction.[3]

To sense SO$_2$ molecules and to increase energy savings, this study uses a solid electrolyte YSZ film in a SnO$_2$ MEMS structure to form a MEMS SO$_2$ gas sensor. The properties of the fabricated sensors are also determined. The sensing properties of the YSZ thin film SO$_2$ gas sensor are determined.

Experimental

Fig. 1(a) schematically depicts the processing steps for the YSZ/SnO$_2$ MEMS SO$_2$ gas sensor and Fig. 1(b) shows the structure of the YSZ/SnO$_2$ MEMS SO$_2$ gas sensor. The structure comprises a suspension, an isolation layer, a micro heater and a sensing material. The micro heater provides a heat source that generates temperatures up to 450 °C. Recently, the authors reported the fabrication of a MEMS SO$_2$ gas sensor structure.[9] This study uses a different micro heater material, interdigital transducer (IDT) electrode (Ni/Cr) and sensing film (YSZ/SnO$_2$). Prior to the fabrication of an YSZ/SnO$_2$ MEMS SO$_2$ gas sensor, a 6 inch Si wafer was thermally oxidized to form a 700 nm-thick SiO$_2$ film. Standard photolithography was used to define the micro heater and the IDT electrode and a 50 nm thick Cr adhesion layer was deposited on a SiO$_2$/Si substrate. A 300 nm Ni film was then deposited on the Cr/SiO$_2$/Si substrate using electron

[a]Department of Electronic Engineering, National Kaohsiung University of Science and Technology, Kaohsiung 807, Taiwan. E-mail: tj.hsueh@gmail.com

[b]Institute of Microelectronics, Department of Electrical Engineering, National Cheng Kung University, Tainan 701, Taiwan
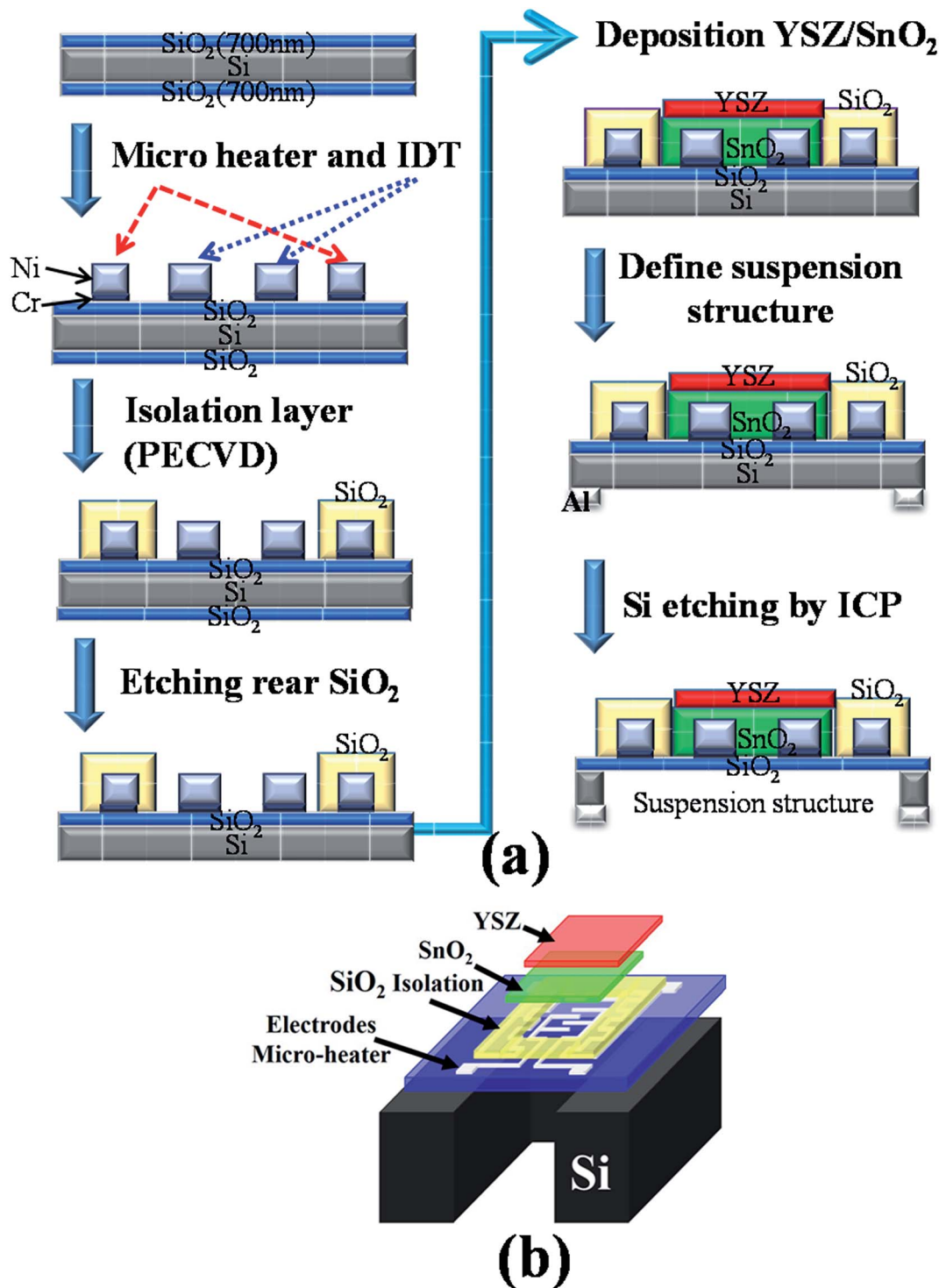
Fig. 1 (a) A schematic diagram of the processing steps for the YSZ/SnO$_2$ MEMS SO$_2$ gas sensor and (b) the structure of the YSZ/SnO$_2$ MEMS SO$_2$ gas sensor.

gun evaporation. A 400 nm SiO$_2$ was deposited on the micro heater using PECVD.

For the sensor film, a 600 nm thick SnO$_2$ layer and a 300 nm thick YSZ layer were deposited by sputtering. Acetone was used to remove the positive type photoresist.

Finally, on the reverse side, a 200 nm thick Al layer was then deposited as the etching barrier layer by sputtering. Standard photolithography was used to make a mask to etch the Al layer. Acetone was used to remove the positive-type photoresist and the exposed Al was then wet-etched using

aluminum etch. For the DRIE process, the flow rates for SF_6 gas and O_2 gas, the substrate temperature, the etching time, the electrode gap, the RF power and the chamber pressure were set at 6.3 sccm, 70 sccm, −120 °C, 210 min, 7 cm, 1000 W, and 10 mTorr, respectively.

The thermal image and morphology were measured using a thermal imaging camera and field-emission scanning electron microscopy (FESEM, JEOL JSM-7000F). The crystallographic properties of the as-grown samples were then determined using X-ray diffraction (XRD; MXP18, and MAC Science) measurements. The resulting gas sensor was then electronically characterized using a Keithley 2400 source meter and a personal computer.

Results and discussion

Fig. 2(a) shows the top view SEM images of the YSZ/SnO₂ MEMS SO₂ gas sensor. It is found that the morphology of the surface is the same as that in Fig. 1(b). Fig. 2(b) shows the top optical microscopy image of the YSZ/SnO₂ MEMS SO₂ gas sensor. It was found that the annular micro-heater surrounds the finger-like

electrodes. The inset of Fig. 2(a) shows an enlarged image of the sensing film (green dotted circle). It is seen that the YSZ has a uniform grain size, with a diameter of about 50 nm. It is also seen that there is a gap between each grain of at most 20 nm. These interfaces create oxygen diffusion pathways for gas sensing.[10]

Fig. 3 shows the crystalline properties of YSZ films from their XRD patterns. YSZ films were deposited on a SnO₂/SiO₂/Si substrate using the sputtering parameters, without thermal treatment. The (111), (200), (220), and (311) peaks denote the crystallization planes of YSZ (JCPDS 30-1468). The (111) is the main growth plane.

A resistive heater operates on the metal wire thermal principle. Fig. 4(a) shows infrared thermal images of the YSZ/SnO₂ gas sensor. There is a temperature difference between the micro heater (red square) and the suspension structure (red dashed lines). The other area is also approximately at room temperature because the micro heater provides a heat source and the suspension structure prevents thermal diffusion. The temperature of the sensing film is approximately 201 °C, 251 °C, 297 °C, 350.6 °C and 400 °C when the current in the micro-heater is approximately 33 mA, 37 mA, 39 mA, 42 mA and 44 mA, respectively, as shown in Fig. 4(b). The current increase linearly as the temperature is increased. When the temperature of the sensing film is 201 °C, 251 °C, 297 °C, 350.6 °C, and 400 °C, the required power is 103 mW, 136 mW, 164 mW, 197 mW, and 229 mW, respectively.

Fig. 5 shows the detector sensor responses for three SO₂ gas sensors, measured at 400 °C. During these measurements, 250 ppb SO₂ gas was introduced into a sealed chamber and the resistivity of the sensor was measured in air (R_a) and in the presence of SO₂ gas (R_b). To quantify the sensor's performance, the response of this sensor is $[((R_a - R_b)/R_a) \times 100\%]$.[11] This definition gives a sensor response of 16% for the YSZ/SnO₂ sensing film with the MEMS structure (micro-heater and
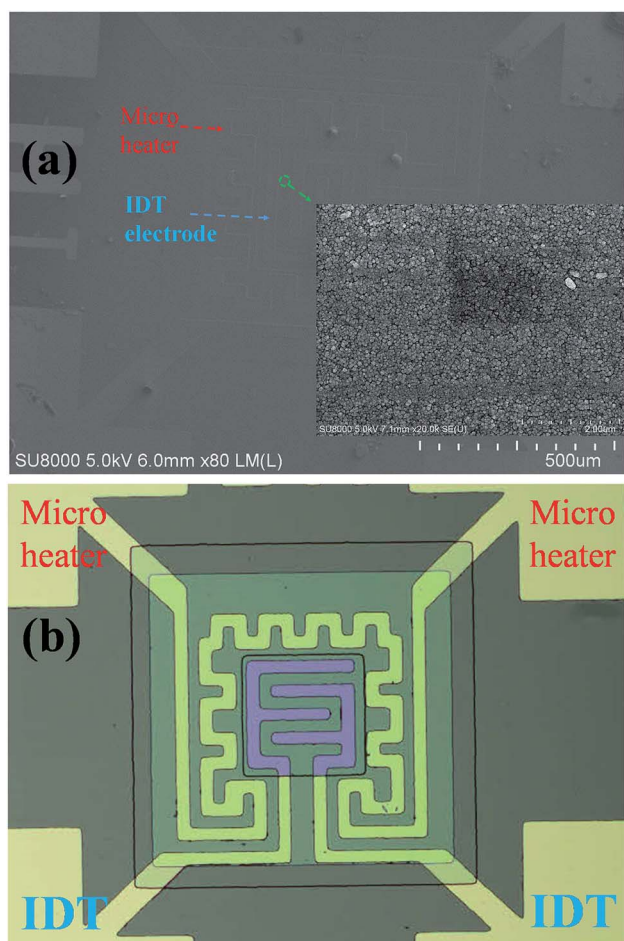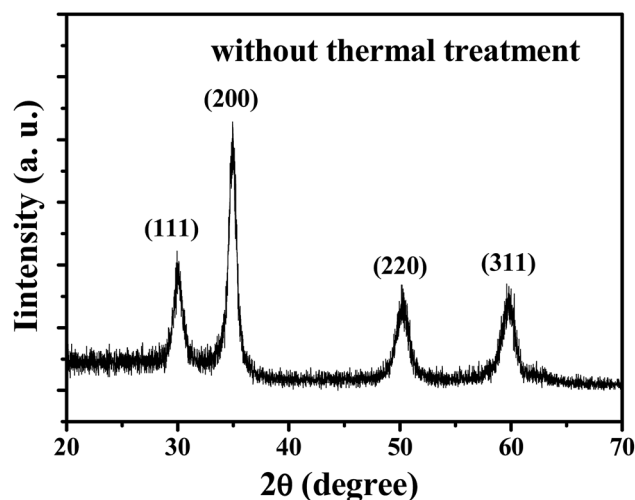

Fig. 2 (a) The top view SEM images of the YSZ/SnO₂ MEMS SO₂ gas sensor. The inset shows an enlarged image of the sensing film (green dotted circle). (b) The top optical microscopy image of the YSZ/SnO₂ MEMS SO₂ gas sensor.

Fig. 3 The XRD patterns for YSZ films: YSZ films were deposited on a SnO₂/SiO₂/Si substrate.
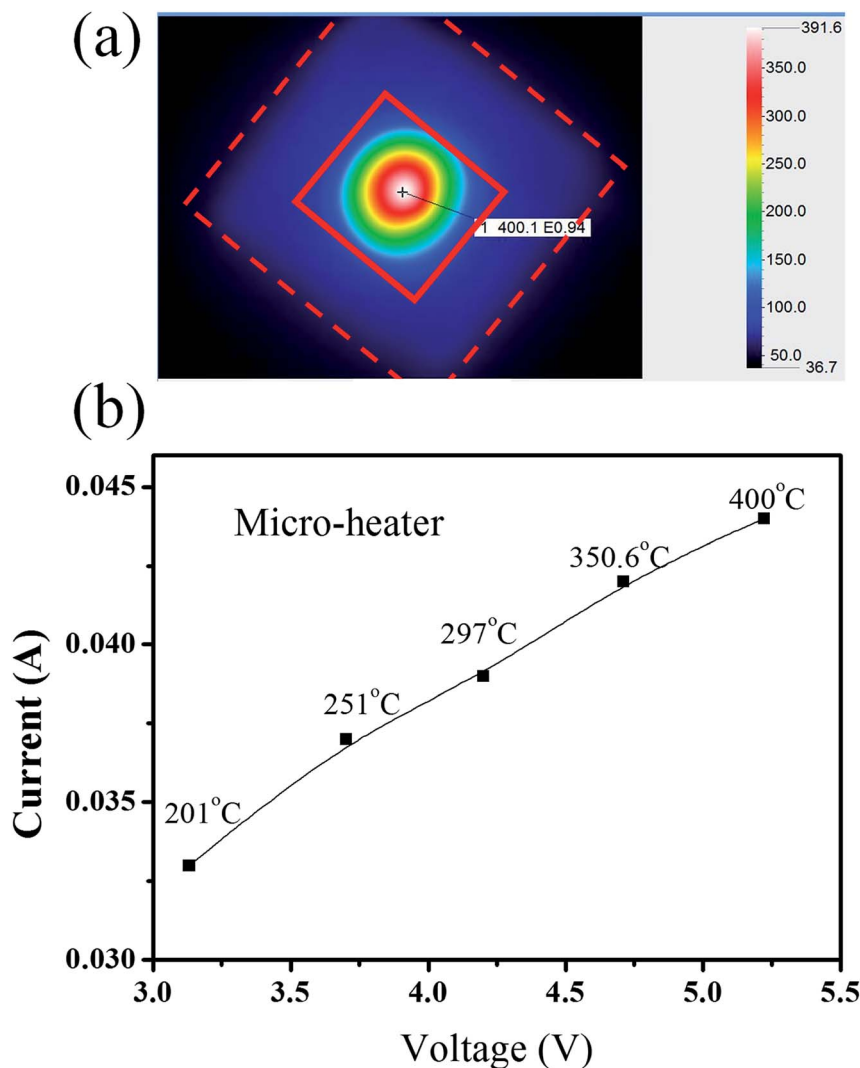
Paper

Fig. 4 (a) Infrared thermal images of the YSZ/SnO$_2$ gas sensor and (b) the temperature of the sensing film.

suspending structure). The sensor response is only around 10% for the pure SnO$_2$ thin film. In other words, the sensitivity to SO$_2$ gas is significantly increased by the deposition of YSZ
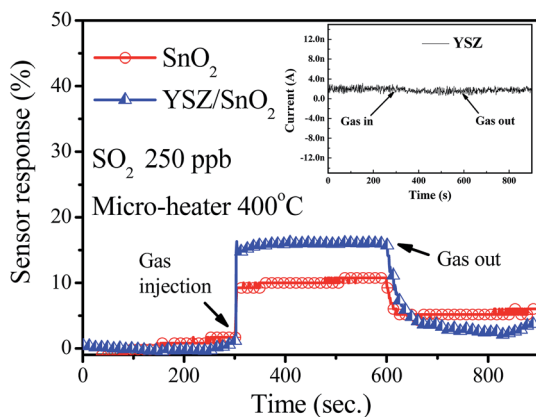

Fig. 5 Detector sensor responses for various SO$_2$ gas sensors, measured at 400 °C. The inset in Fig. 4 shows that the sensor response for the sample with only the YSZ film.

film on the SnO$_2$ thin film surface. A sample with only the YSZ thin film was prepared and the same SO$_2$ gas sensing measurement at 400 °C was performed. The inset in Fig. 5 shows that the sensor response for the sample with only the YSZ film is a null response. This result shows that the large 16% sensor response is attributable to the SnO$_2$ thin film with YSZ film (YSZ/SnO$_2$). It has been reported that the SnO$_2$ can be used to sense toxic gas with low sensitivity at higher temperatures.[10,12] In terms of the sensing mechanism for a YSZ/SnO$_2$/MEMS SO$_2$ sensor, the YSZ thin film allows the redox reaction and the SnO$_2$ thin film acts as an electronic transmission path. As shown in Fig. 6(a), when the YSZ/SnO$_2$/MEMS SO$_2$ sensor is surrounded by air, oxygen molecules are adsorbed onto the YSZ surface and capture electrons from the sensing thin film to generate chemisorbed oxygen species (O_2^-, O^{2-}, O^-). Therefore, the sensor becomes highly resistive. When SO$_2$ gas is introduced, the sensor is exposed to traces of reductive gas. The reductive gas reacts with the oxygen species on the YSZ surface and the concentration of oxygen species on the YSZ surface is reduced, so the concentration of electrons is
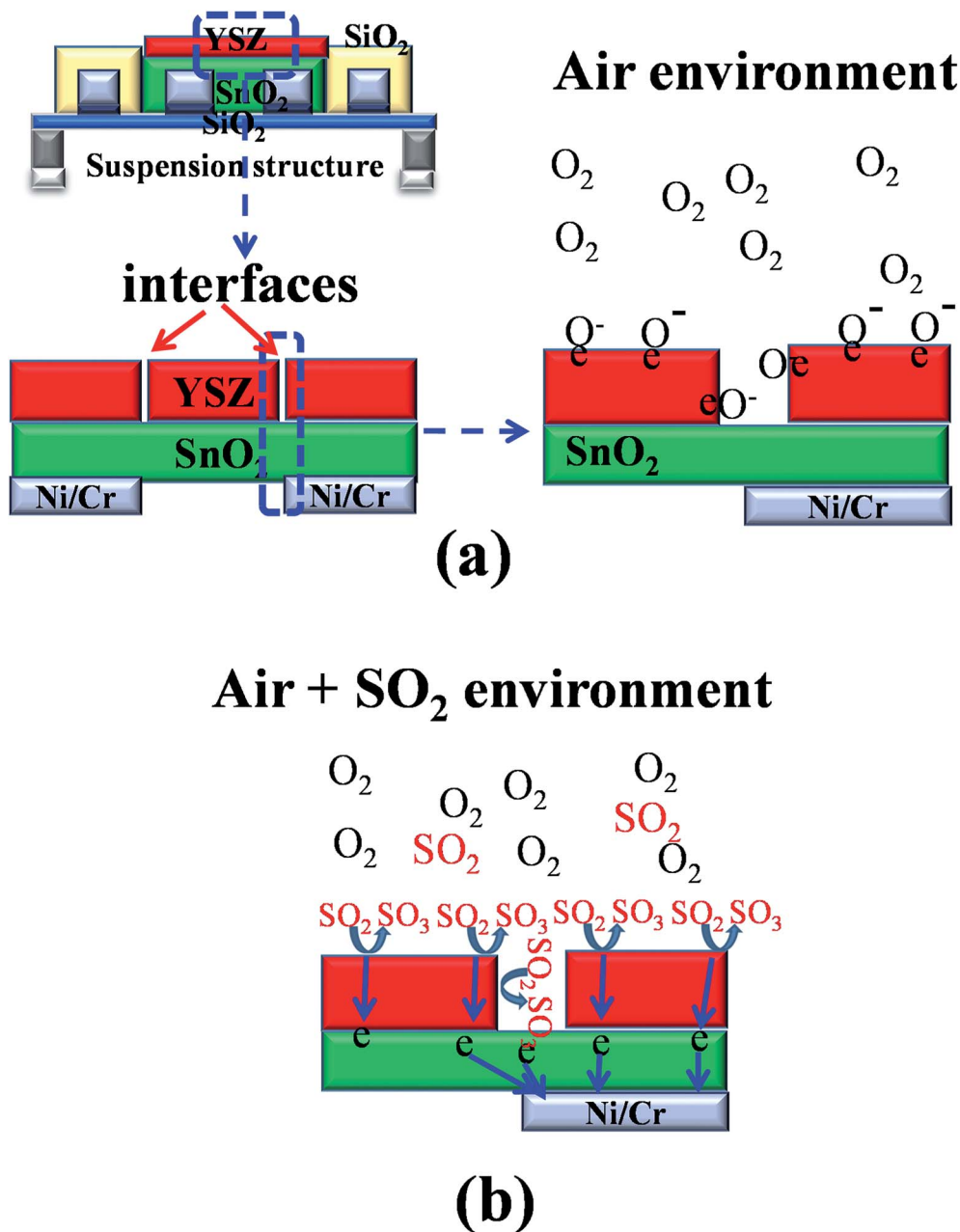
Fig. 6 Schematic diagram of a YSZ/SnO$_2$/MEMS SO$_2$ sensor surrounded by (a) air and (b) SO$_2$ gas.

increased, as shown in Fig. 6(b) and the sensor becomes more conductive.

Fig. 7 shows the sensor response of the YSZ/SnO$_2$/MEMS sensor measurement various gases at 400 °C. It was found that the measured response is around 16% and 6% when the concentration of injected SO$_2$ and H$_2$S gas is 250 ppb, respectively. It also was found that the sensor response of YSZ/SnO$_2$/MEMS sensor is not obvious when the concentration of NH$_3$ and NO$_2$ gases are 250 ppb, respectively. The measured results was shown that the YSZ/SnO$_2$/MEMS sensor is more responsive to sulfide; especially SO$_2$ gas.[10]

Fig. 8 shows the variation in sensor response variations for a YSZ/SnO$_2$/MEMS SO$_2$ sensor when it is exposed to pumped SO$_2$ gas. These measurements were performed by injecting various amounts of SO$_2$ gas into the sealed chamber, followed by pumping at 400 °C (micro-heater). Using the same definition, the measured response is around 16%, 23%, 27% and 31% when the concentration of injected SO$_2$ gas is 250 ppb, 500 ppb, 750 ppb and 1000 ppb, respectively. In other words, the sensor response increases when the SO$_2$ gas concentration increases. The measured device resistivity also responds rapidly when SO$_2$ is injected gas into the chamber and pumped away. This result shows that the fabricated sensor responds rapidly.

Fig. 9(a) shows the sensor response for the YSZ/SnO$_2$ sensor at various temperatures. It should be noted that only 250 ppb
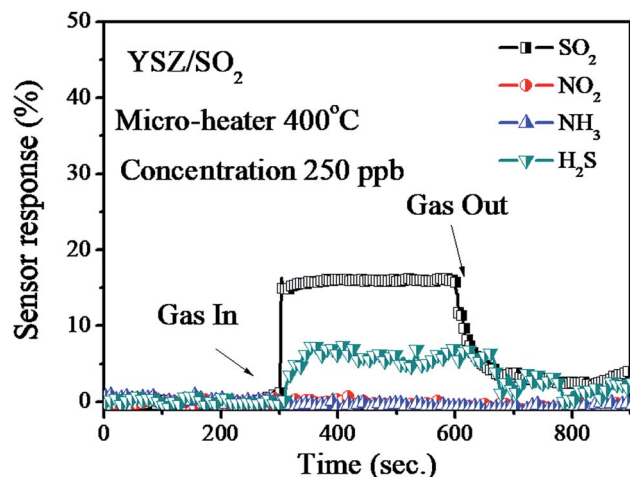
Fig. 7 The sensor response for the YSZ/SnO₂/MEMS sensor to various gases at 400 °C.
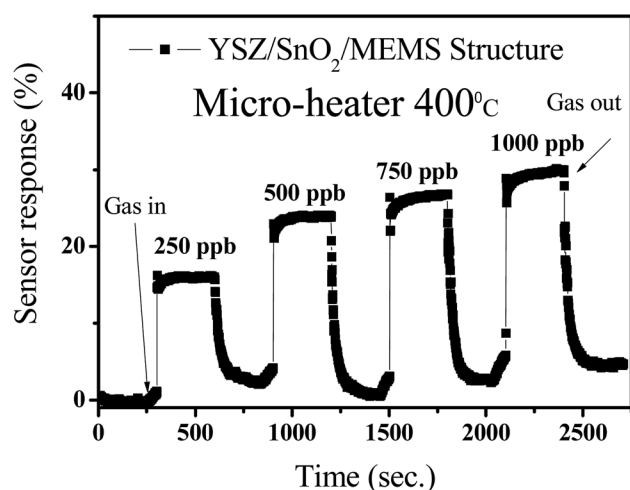

Fig. 8 The variation in sensor response for the YSZ/SnO₂/MEMS sensor material when SO₂ gas is injected and pumped.

SO₂ gas was injected into the chamber for these measurements. The measured responses are around 6%, 45%, 20% and 16% when the sensor is operated at 250 °C, 300 °C, 350 °C and 400 °C, respectively. In other words, sensor response increases initially, reaches a maximum at 300 °C and then begins to decrease as the operational temperature is increased from 250 to 400 °C. At low temperatures, the poor sensor response is attributed to the fact that SO₂ molecules do not have enough thermal energy to react with the surface-adsorbed oxygen species. However, the reduction in sensor response above 300 °C is attributed to the difficulty of exothermic SO₂ gas adsorption.[11] This result is similar to that of the study by Duan *et al.*[13] To verify the reproducibility of the YSZ/SnO₂/MEMS SO₂ sensors, three good samples were randomly produced using the same wafer, as shown in Fig. 9(b). It is seen that the results are reproducible with an inaccuracy of ±5%. These values show that the sensor that is proposed by this study has many applications.
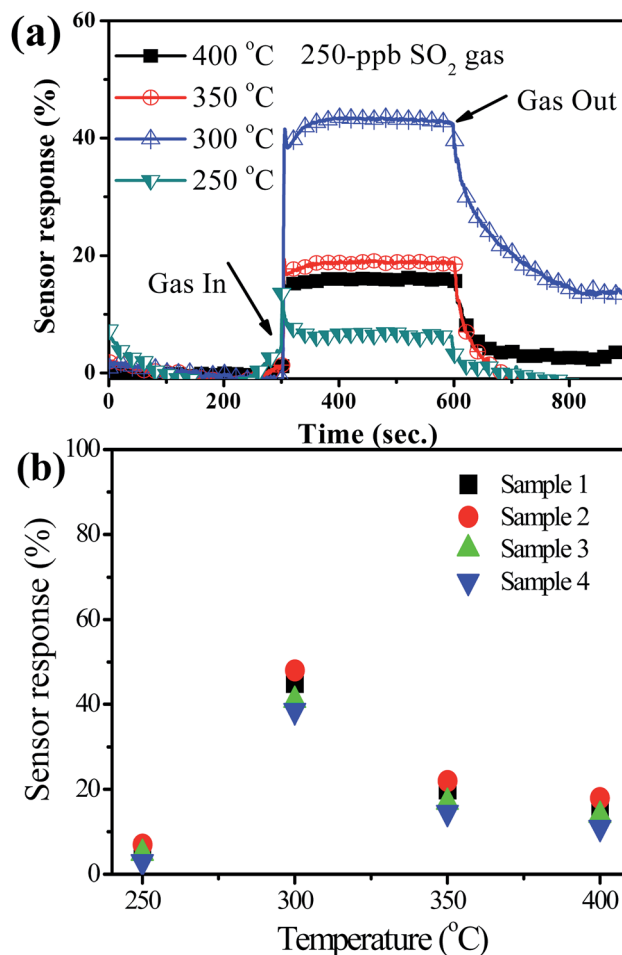

Fig. 9 (a) Sensor response for the YSZ/SnO₂ sensor at various temperatures and. (b) Five of the same samples at various temperatures (including the sensor of (a)).

Conclusion

In summary, YSZ film is deposited by RF sputtering into a SnO₂ MEMS SO₂ gas sensor to form a YSZ/SnO₂ MEMS SO₂ gas sensor. XRD analysis shows the presence of (111), (200), (220), and (311) peaks that denote the crystallization planes of YSZ. Compared with a SnO₂ MEMS SO₂ gas sensor and a YSZ MEMS SO₂ gas sensor, a YSZ/SnO₂ MEMS SO₂ gas sensor has the best sensor response when the sensors are at 400 °C and in 250 ppb SO₂ gas ambience. The measured responses for the YSZ/SnO₂ sensor are also around 6%, 45%, 20% and 16% when the sensor is operated at 250 °C, 300 °C, 350 °C and 400 °C, respectively.

Conflicts of interest

There are no conflicts to declare.

Acknowledgements

B10708); Center for Intelligent Machines and Smart Materials; Taiwan Semiconductor Research Institute.

References

1 E. Stokstad, Ammonia pollution from farming may exact hefty health costs, *Science*, 2014, **343**, 238.

2 Y. Zhao, L. Duan, J. Xing, T. Larssen, C. P. Nielsen and J. M. Hao, Soil acidification in China: is controlling SO_2 emissions enough, *Environ. Sci. Technol.*, 2009, **43**, 8021–8026.

3 Y. Liu, X. Xu, Y. Chen, Y. Zhang, X. Gao, P. Xu, X. Li, J. Fang and W. Wen, An integrated micro-chip with $Ru/Al_2O_3/ZnO$ as sensing material for SO_2 detection, *Sens. Actuators, B*, 2018, **262**, 26–342.

4 M. L. Yin, Y. Yao, H. B. Fan and S. Z. Liu, WO_3-SnO_2 nanosheet composites: Hydrothermal synthesis and gas sensing mechanism, *J. Alloys Compd.*, 2018, **736**, 322–331.

5 C. Schwandta, R. V. Kumara and M. P. Hills, Solid state electrochemical gas sensor for the quantitative determination of carbon dioxide, *Sens. Actuators, B*, 2018, **265**, 27–34.

6 F. C. Antunes, C. A. Goulart, M. R. B. Andreeta and D. P. F. de Souza, YSZ/Al_2O_3 multilayer thick films deposited by spin coating using ceramic suspensions on Al_2O_3 polycrystalline substrate, *Mater. Sci. Eng., B*, 2018, **228**, 60–66.

7 C. L. Lu, S. J. Changa, T. C. Weng and T. J. Hsueh, A Bifacial SnO_2 thin film Ethanol Gas Sensor, *IEEE Electron Device Lett.*, 2018, **39**, 1223–1225.

8 P. Mitra, A. P. Chatterjee and H. S. Maiti, ZnO thin film sensor, *Mater. Lett.*, 1998, **35**, 33–38.

9 C. H. Lin, S. J. Chang and T. J. Hsueh, A WO_3 Nanoparticles NO Gas Sensor Prepared by Hot-Wire CVD, *IEEE Electron Device Lett.*, 2017, **38**, 266–269.

10 C. A. Betty and S. Choudhury, Charge carrier transport in nanocrystalline SnO2 thin film sensor and temperature dependence of toxic gas sensitivity, *Sens. Actuators, B*, 2016, **237**, 787–794.

11 S. J. Chang, T. J. Hsueh, I.-C. Chen and B. R. Huang, Highly sensitive ZnO nanowire CO sensors with the adsorption of Au nanoparticles, *Nanotechnology*, 2008, **19**, 175502–175506.

12 A. Cirera, A. Vila, A. Diéguez, A. Cabot, A. Corne and J. R. Morante, Microwave processing for the low cost, mass production of undoped and in situ catalytic doped nanosized SnO_2 gas sensor powders, *Sens. Actuators, B*, 2000, **64**, 65–69.

13 Z. Duan, Y. Zhang, Y. Tong, H. Zou, J. Peng and X. Zheng, Mixed-Potential-Type Gas Sensors Based on Pt/YSZ Film/$LaFeO_3$ for Detecting NO_2, *J. Electron. Mater.*, 2017, **46**, 6895–6900.